Faculty of Science
UNIVERSITY OF COPENHAGEN

December 2, 2018

Investigating stability properties for characteristic electric power systems based on a heuristic classification-scheme

Lars Reiter Nielsen

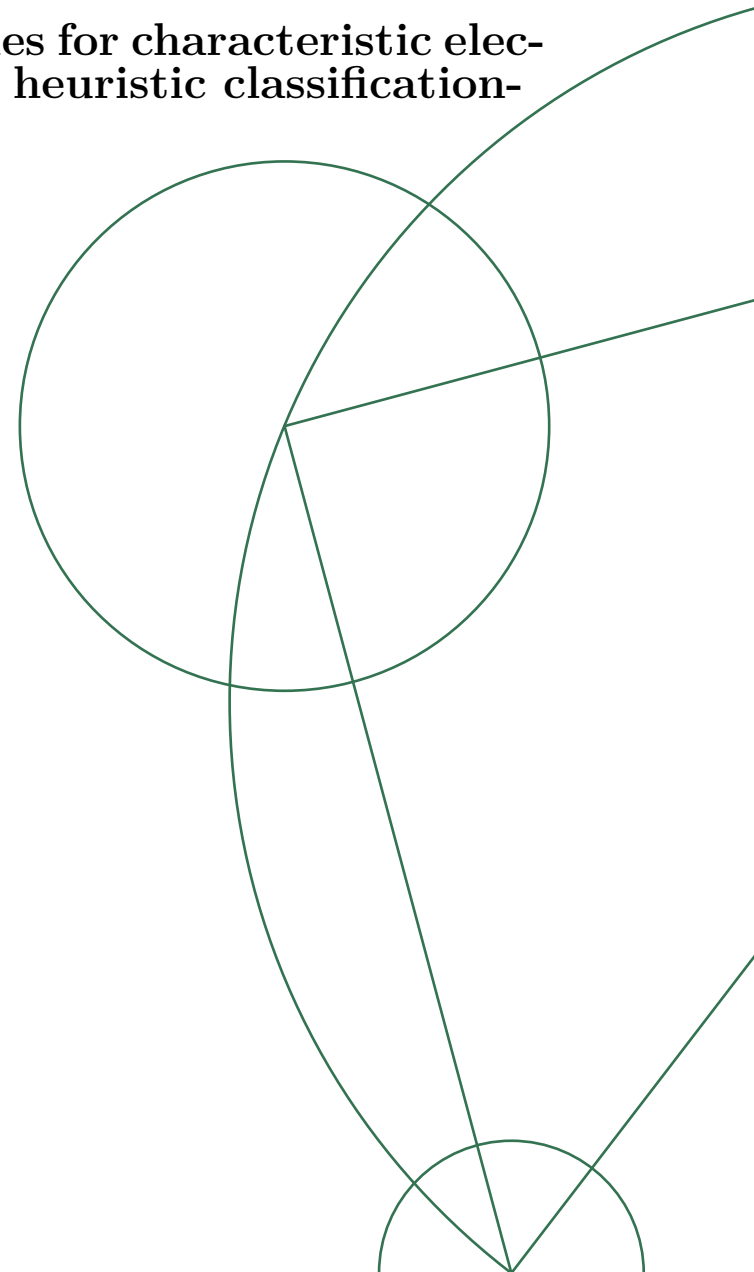

Master thesis

Advisor: Peter Ditlevsen

Abstract

In a world striving for sustainability and a greener future, various initiatives have been set into motion. Remaking and rethinking the electric power system is such an example, where the mounting of many new distributed energy sources adds a new layer of complexity, since distributed sources are autonomous in nature. Synchronization of a power grid is essential for the grid to function, and so the question is how the stability of future grids can be assured. In this study we will use a Kuramoto like model to analyse the dynamics of power grids. These power grids will be constructed using a heuristic which takes into account the distribution of large and small consumers and generators. The heuristic generates 12 different power grid types, which are analysed in terms of dynamical and transient stability. We confirm previously reported stability criteria, namely that decentralization increases dynamic stability and unveil similarities and differences between the 12 grid types in terms of stability.

Contents

1 Introduction **3**
1.1 The Kuramoto model 3

2 Characterising quasi-isomorphic topologies **5**
2.1 Heuristic classification scheme 8
2.2 Defining small to large power generation and consumption 9
2.3 Measure normal operation and check for steady state 10
2.4 Determine critical coupling strength 11

3 Assessing stability characteristic of Type motifs **12**
3.1 Measuring dynamic stability 12
3.2 Measuring transient stability 12
3.3 Simulation range using error analysis 14

4 Numerical results **17**
4.1 Dynamical stability analysis 17
4.2 Transient stability analysis 20

5 Discussion and outlook **22**

Appendix A Constructing Quasi-isomorphic topologies **23**

Appendix B Deriving the grid model **24**

Appendix C Visualizing grid types **26**

1 Introduction

This century marks a critical stage in the Earths history, where we are faced with global challenges on a scale that forces the world society to act promptly if we are to save our common home from impoverishment and unwanted climate effects. This is no easy mission, as it requires the unification of all nations, and in particular it demands the adherence of the influential political leaders and the commitment of the larger nations. The Paris Agreement is an example of a collaboration of nearly 200 nations working together to mitigate global warming and climate changes which is taking its toll on our Earth. This agreement incites a green and sustainable transition within the ratifying countries and here among also a change in their respective electrical power grid, where windmill parks, photovoltaic power stations, hydroelectricity solutions and other forms of renewable energy sources will take the place of the contemporary power plants which runs on fossil fuels, such as coal or natural gas.

In Denmark, the future offers the prospect of smart households featuring solar panels, heat pumps, micro-CHP's and other smart electric units all connected to the power grid which consequently leads to a much more complex grid with numerous autonome power generators [16]. Because active control is now less viable, it begs the question how the power grid will behave on its own. This has been the focus of several studies [2, 10, 11, 12, 13, 14, 15], where stability issues has been answered by modelling the entire network as a undirected graph with nodes (consumers and generators) representing synchronous motors. These rotating machines (or oscillators) can for instance be visualized as water turbines or electric motors with their own frequency. The mathematical model used to describe this is named the Kuramoto model (see 1.1) and has been a popular choice modelling complex dynamical systems in many fields, particularly in biology.

The different studies uncovered many aspects of the dynamics of future power grids. One study gave insight as to how geometric frustration can promote Braess Paradox in power systems if line capacity is changed or if new links are added (or removed) [11]. Other studies made use of a linear analysis to study how robust a future grid would be against small perturbations [12][13] and another study examined how (larger) long-term pertubations affects synchrony of the grid using a non-linear stability analysis [10].

A common focus was to examine optimum grid structure. In this study, we will continue that focus, but by considering different *groups* or *classes* of grids (to be defined) and performing a stability analysis of each class in order to discuss their robustness both isolated and relative to the other classes.

We will use generator and consumer units which are scaled to match the Danish power grid (in proportion), such that the largest consumers (huge consumers) correspond to the largest city in Denmark and the largest generators (huge generators) corresponds to the largest windmill parks (more of this later).

1.1 The Kuramoto model

As mentioned, the grid of the future offers less active control since for instance wind and solar energy are volatile sources of energy. In the light of this it makes sense to investigate how the grid performs without regulation. To this purpose we will introduce a model, which has drawn a lot of attention in this field, namely the *Kuramoto model* with the governing (coupled)

differential equation(s):

$$\underbrace{\frac{\mathrm{d}^2\phi_j(t)}{\mathrm{d}t^2}}_{\sim \text{ accumulation}} = \underbrace{P_j}_{\sim \text{ source}} - \underbrace{\alpha_j \frac{\mathrm{d}\phi_j(t)}{\mathrm{d}t}}_{\sim \text{ dissipation}} + \sum_{i=1}^{N} \underbrace{\mathrm{K}_{ij} \sin(\phi_i(t) - \phi_j(t))}_{\sim \text{ transferred}} \qquad j \in \{1, ..., N\} \tag{1}$$

Here ϕ_j is the phase deviation of oscillator j relative to the grid reference phase, P_j is a composed quantity linearly dependent on the generated/consumed power at oscillator j, α_j is the dissipation coefficient related to the friction of the oscillator unit j (this could for instance be a certain electric motor), K_{ij} describes the line capacity between oscillator i and j and we have $\mathrm{K}_{ij} = 0$ if no line exists. The last term thus contains information about the transfered power and is proportional to the sine of the phase difference of the oscillators. Finally N denotes the total number of oscillators in the grid. For a full derivation and explanation, we refer to appendix B.

For simplicity, we will assume throughout this study that $K_{ij} \equiv K$ for all i, j where a line exists between i and j, such that all lines have the same capacity. Furthermore we will only consider one type of (idealized) oscillator unit, such that the dissipation coefficient is a constant $a_j \equiv a$ for all j.

During normal operation where all consumers and generators runs in synchrony there exist a phase-locked state where $\frac{\mathrm{d}^2\phi_j(t)}{\mathrm{d}t^2} = \frac{\mathrm{d}\phi_j(t)}{\mathrm{d}t} = 0$ and $\sum_{i=1}^{N} P_i = 0$. In this case (1) reduces to

$$P_j(t) = \mathrm{K} \sum_{i=1}^{N} \sin(\phi_j(t) - \phi_i(t)) \tag{2}$$

in some cases (2) can be solved analytically, for instance in the elementary case where $N = 2$ with one generator and one consumer we have that $-P_1 = P_2$ and we can rewrite (2)

$$\begin{cases} P_1 = \mathrm{K} \sin(\phi_1(t) - \phi_2(t)) & \text{for } j = 1 \\ -P_1 = \mathrm{K} \sin(\phi_2(t) - \phi_1(t)) & \text{for } j = 2 \end{cases}$$

now we set $P \equiv P_1$ and $\Delta\phi = \phi_1 - \phi_2$ and recognize that the system of equations is degenerate, we thus obtain a single equation $P = \mathrm{K} \sin(\Delta\phi)$ which has the solutions $\Delta\phi_1 = \arcsin(\frac{P}{K})$ and $\Delta\phi_2 = \pi - \arcsin(\frac{P}{K})$ assuming that $P \leq K$ (i.e. the power transferred cannot exceed the line capacity). A further analysis shows that the fix point $\Delta\phi_1$ is locally stable, while $\Delta\phi_2$ is unstable which is visualized in figure 1 [19]. Thus the optimum steady state for which the two-node grid operates is attained when the phase difference of the oscillators is (ideally) $\Delta\phi_1$.

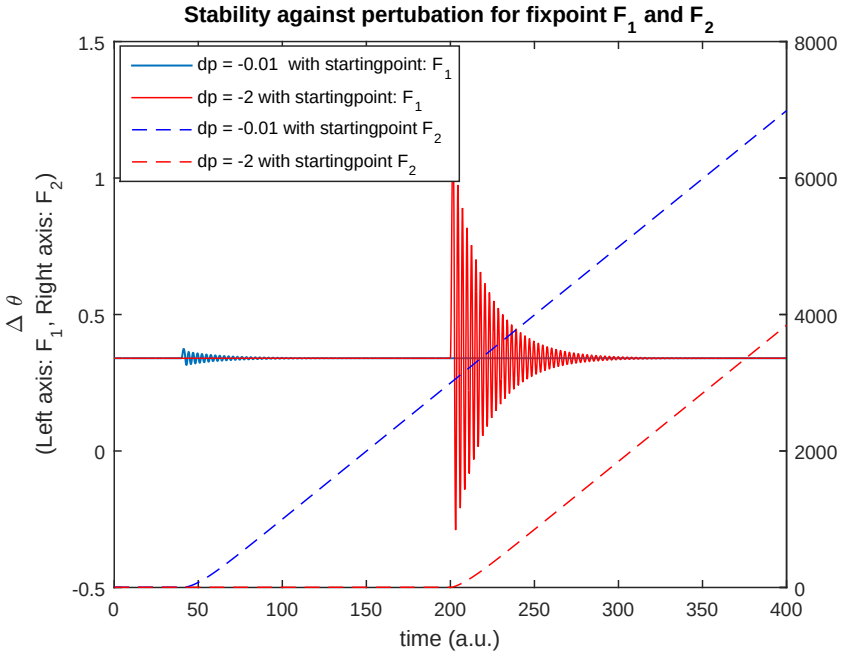

Figure 1: Parameters: Runtime = 500, $\alpha = 0.1$, $\Delta P = 2$, pertubation time duration = 2 units and $(\Delta\theta_0, \Delta\omega_0)^T = F_1$ for solid lines (left-axis) and $(\Delta\theta_0, \Delta\omega_0)^T = F_2$ for dashed lines (right-axis)

2 Characterising quasi-isomorphic topologies

Throughout this study. we will consider networks in which the total power demand is fixed and taken to be $P = 42$ units of power, that is $\sum_{i=1}^{N} |P_i| = 2 \times P$.

These units of power are distributed among tiny consumers (with a power demand P_1^c), small consumers (power demand P_2^c), medium consumers (power demand P_3^c), large consumers (power demand P_4^c) and finally huge consumers (power demand P_5^c).

The total power demand will be supplied by tiny generators (P_1^g), small generators (P_2^g), medium generators (P_3^g), large generators(P_4^g) and huge generators (P_5^g).

The exact values of the power generation (consumption) of the different generators (consumers) will be discussed later.

Now let us define the quantities known as *Consumer-balance-parameters* (CBP) $\mu \equiv (\mu_1, \mu_2, \mu_3, \mu_4, \mu_5)$ and *Generator-balance-parameters* (GBP) $\delta \equiv (\delta_1, \delta_2, \delta_3, \delta_4, \delta_5)$.

The CBP are defined such that μ_i is the fraction of consumers in the grid with a power power demand P_i^c. Similarly the GBP δ_i is the fraction of generators in the grid with a power supply P_i^g. Here i is ranging from 1 to 5 (tiny to huge).

The CBP and GBP together will define the so called 'quasi-isomorphic topologies', which is divided into 4 types:

Type 1: Many small cities, Many small generators:

$$\delta_1, \mu_1 \in \left[\Lambda_1 - \frac{1}{2}\lambda_{12}, \Lambda_1 + \frac{1}{2}\lambda_{12}\right]$$
$$\delta_i \in [\Lambda_i + \sum_{j=1}^{i-1}(-1)^{j+i}\delta_j + (-1)^i\Lambda_1 - \frac{1}{2}\lambda_{i,i+1}, \Lambda_i + \sum_{j=1}^{i-1}(-1)^{j+i}\delta_j + (-1)^i\Lambda_1 + \frac{1}{2}\lambda_{i,i+1}]$$
$$\mu_i \in [\Lambda_i + \sum_{j=1}^{i-1}(-1)^{j+i}\mu_j + (-1)^i\Lambda_1 - \frac{1}{2}\lambda_{i,i+1}, \Lambda_i + \sum_{j=1}^{i-1}(-1)^{j+i}\mu_j + (-1)^i\Lambda_1 + \frac{1}{2}\lambda_{i,i+1}]$$
$$\delta_5 = 1 - \sum_{j=1}^{4}\delta_j \qquad \text{and} \qquad \mu_5 = 1 - \sum_{j=1}^{4}\mu_j$$

for $i = 2, 3, 4$

Type 2: Many small cities, Few large generators:

$$\delta_5, \mu_1 \in \left[\Lambda_1 - \frac{1}{2}\lambda_{12}, \Lambda_1 + \frac{1}{2}\lambda_{12}\right]$$
$$\delta_i \in [\Lambda_i + \sum_{j=i+1}^{5}(-1)^{j+i}\delta_j + (-1)^i\Lambda_1 - \frac{1}{2}\lambda_{i,i+1}, \Lambda_i + \sum_{j=i+1}^{5}(-1)^{j+i}\delta_j + (-1)^i\Lambda_1 + \frac{1}{2}\lambda_{i,i+1}]$$
$$\mu_i \in [\Lambda_i + \sum_{j=1}^{i-1}(-1)^{j+i}\mu_j + (-1)^i\Lambda_1 - \frac{1}{2}\lambda_{i,i+1}, \Lambda_i + \sum_{j=1}^{i-1}(-1)^{j+i}\mu_j + (-1)^i\Lambda_1 + \frac{1}{2}\lambda_{i,i+1}]$$
$$\delta_1 = 1 - \sum_{j=2}^{5}\delta_j \qquad \text{and} \qquad \mu_5 = 1 - \sum_{j=1}^{4}\mu_j$$

for $i = 2, 3, 4$

Type 3: Few large cities, Many small generators:

$$\delta_1, \mu_5 \in \left[\Lambda_1 - \frac{1}{2}\lambda_{12}, \Lambda_1 + \frac{1}{2}\lambda_{12}\right]$$
$$\delta_i \in [\Lambda_i + \sum_{j=1}^{i-1}(-1)^{j+i}\delta_j + (-1)^i\Lambda_1 - \frac{1}{2}\lambda_{i,i+1}, \Lambda_i + \sum_{j=1}^{i-1}(-1)^{j+i}\delta_j + (-1)^i\Lambda_1 + \frac{1}{2}\lambda_{i,i+1}]$$
$$\mu_i \in [\Lambda_i + \sum_{j=i+1}^{5}(-1)^{j+i}\mu_j + (-1)^i\Lambda_1 - \frac{1}{2}\lambda_{i,i+1}, \Lambda_i + \sum_{j=i+1}^{5}(-1)^{j+i}\mu_j + (-1)^i\Lambda_1 + \frac{1}{2}\lambda_{i,i+1}]$$
$$\delta_5 = 1 - \sum_{j=1}^{4}\delta_j \qquad \text{and} \qquad \mu_1 = 1 - \sum_{j=2}^{5}\mu_j$$

for $i = 2, 3, 4$

Type 4: Few large cities, Few large generators:

$$\delta_5, \mu_5 \in \left[\Lambda_1 - \frac{1}{2}\lambda_{12}, \Lambda_1 + \frac{1}{2}\lambda_{12}\right]$$

$$\delta_i \in [\Lambda_i + \sum_{j=i+1}^{5} (-1)^{j+i}\delta_j + (-1)^i\Lambda_1 - \frac{1}{2}\lambda_{i,i+1}, \Lambda_i + \sum_{j=i+1}^{5} (-1)^{j+i}\delta_j + (-1)^i\Lambda_1 + \frac{1}{2}\lambda_{i,i+1}]$$

$$\mu_i \in [\Lambda_i + \sum_{j=i+1}^{5} (-1)^{j+i}\mu_j + (-1)^i\Lambda_1 - \frac{1}{2}\lambda_{i,i+1}, \Lambda_i + \sum_{j=i+1}^{5} (-1)^{j+i}\mu_j + (-1)^i\Lambda_1 + \frac{1}{2}\lambda_{i,i+1}]$$

$$\delta_1 = 1 - \sum_{j=2}^{5} \delta_j \qquad \text{and} \qquad \mu_1 = 1 - \sum_{j=2}^{5} \mu_j$$

for $i = 2, 3, 4$

where $\Lambda \equiv \{\Lambda_1, \Lambda_2, \Lambda_3, \Lambda_4, \Lambda_5\} = \{0.5, 0.2, 0.15, 0.1, 0.05\}$ and $\lambda \equiv \{\lambda_{12}, \lambda_{23}, \lambda_{34}, \lambda_{45}\} = \{0.2, 0.1, 0.1, 0.05\}$ are fixed arrays.

To visualize the construction, we refer to figure 2. For further details, see appendix A. See also appendix C for instances of grid realizations.

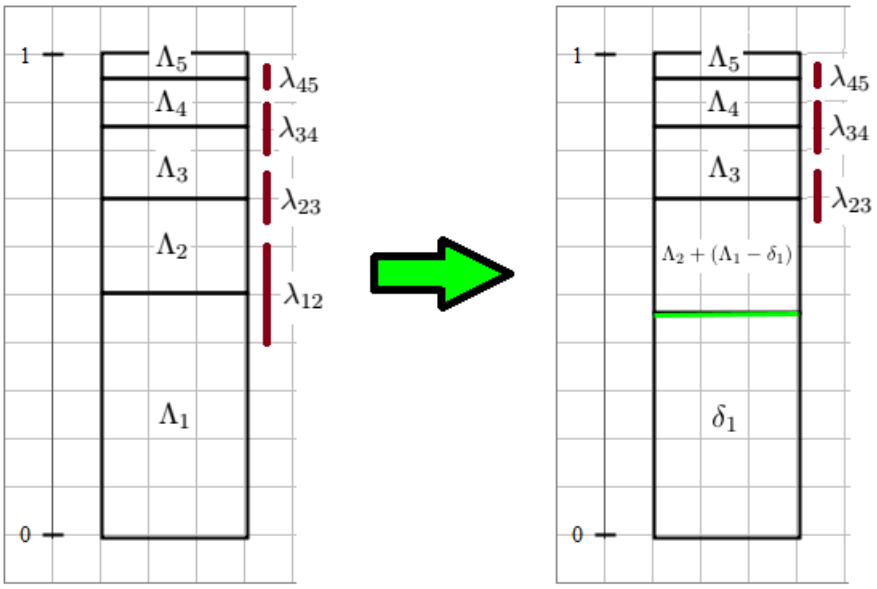

Figure 2: First δ_1 is randomly selected from the interval $[\Lambda_1 - \frac{1}{2}\lambda_{12}, \Lambda_1 + \frac{1}{2}\lambda_{12}]$. The selection of δ_1 increases the interval from which δ_2 can be drawn by an ammount $\Lambda_1 - \delta_1$.

With this convention, the average GBP $\bar{\delta}$ and CBP $\bar{\mu}$ of type 1 (say) is found to be

$$\bar{\delta} \equiv (\bar{\delta_1}, \bar{\delta_2}, \bar{\delta_3}, \bar{\delta_4}, \bar{\delta_5}) = \Lambda = (\bar{\mu}_1, \bar{\mu}_2, \bar{\mu}_3, \bar{\mu}_4, \bar{\mu}_5) \equiv \bar{\mu} \tag{3}$$

Notice the spelling 'few large'. This signals that the total power is distributed among only few units, thus the size of the network is smaller compared to types with 'many small'. The largest networks are found in the type 1 category whereas the smallest are found to be type 4.

2.1 Heuristic classification scheme

With the CBP and GBP chosen according to the relevant type, the power grid is constructed as follows:

Let N_i^c be the total number of consumers of size i (defined similar to the power quantities), and let N_i^g be the total number of generators of size i.

Now let $N^c \equiv \sum_{i=1}^5 N_i^c$ and $N^g \equiv \sum_{i=1}^5 N_i^g$ be the total consumers and generators respectively. We might approximate these quantities with the following convex combinations

$$N^c \approx \sum_{i=1}^{5} \mu_i \cdot \frac{P}{P_i^c} \qquad \text{and} \qquad N^g \approx \sum_{i=1}^{5} \delta_i \cdot \frac{P}{P_i^g} \tag{4}$$

where the i'th term of each sum represents the number of generators/consumers of the respective size (that is N_i^g or N_i^c) .

The problem with the above construction is that one or more of these terms could be a fraction, and we require N_i^c and N_i^g to be whole numbers for our construction to be sensible.

To remedy this, we instead let $N_i^c = \lfloor \mu_i \cdot \frac{P}{P_i^c} \rfloor$ and $N_i^g = \lfloor \mu_i \cdot \frac{P}{P_i^c} \rfloor$ where $x \mapsto \lfloor x \rfloor$ is the floor function.

Now in a synchronous power grid, there must be balance in power demand and production:

$$\sum_{i=1}^{5} P_i^c N_i^c \stackrel{!}{=} \sum_{i=1}^{5} P_i^g N_i^g \tag{5}$$

To ensure this is upheld we define the rescale parameter

$$\beta = \frac{\sum_{i=1}^5 P_i^c N_i^c}{\sum_{i=1}^5 P_i^g N_i^g}$$

And then adjust the power consumption accordingly $P_i^g \to \beta P_i^g$.

Modern power grids have an average degree of approximately $\hat{d} = 2.7$ [2, p. 3]. We will adopt this into our construction, therefore the total number of edges E that we need to distribute among our $N^c + N^g$ oscillators are given as

$$E = \frac{(N^c + N^g) \times 2.7}{2}$$

where the factor $\frac{1}{2}$ exists because one edge adds one local degree at each connected node. This also shows that unless $(N^c + N^g) \times 2.7$ takes on some even integer value, the number of edges will be a fraction. The quick fix will be to simply define

$$E := \lfloor \frac{(N^c + N^g) \times 2.7}{2} \rfloor$$

where we once again use the floor function. The average degree will then be approximately $\hat{d} = 2.7$ which is good enough.

Notice that following this construction, the sparsity of the graph (representing the power grid) will not be adjustable. Instead we will add three suffixes onto our types defined above:

Type i-C : **C**omplete connected power grid of type i

Type i-U : **U**niform connected power grid of type i

Type i-R : **R**andom connected power grid of type i

For C types, the graph does not contain any dead ends which was in previous studies coupled to a decrease in synchrony [10]. The network is represented by a biconnected graph, meaning that the graph has no articulation nodes (nodes that can be removed without disconnecting other nodes). In this sense, the network is complete.

For U types, the edges are distributed uniformly in the grid. This means that each oscillator has a local degree of approximately $\frac{E}{N^g+N^c}$. Approximately, because the mean value might be a fraction, in which case there will be nodes (proprtional to the remainder of the division) with one more edge. In the case where $\frac{E}{N^g+N^c} \geq 2$ this graph exhibit no dead ends.

For R types, the edges are connected randomly in the grid.

2.2 Defining small to large power generation and consumption

In this study we will attempt to mirror the danish power consumption and production.

Initially we will set the power consumption of the medium consumers to unity, i.e. $P_3^c = 1$.

Now we will adopt the following convention (in the attempt to reflect the danish city scale [9])

- Tiny consumers represents cities of roughly 10000 citizens
- Small consumers represents cities of roughly 25000 citizens
- Medium consumers represents cities of roughly 50000 citizens
- Large consumers represents cities of roughly 100000 citizens
- Huge consumers represents cities of roughly 350000 citizens [1]

Now we might expect the power consumption to scale proportionally with the number of citizens (of a given city), not only because of the increase in households, but also because larger cities tend to be more industrialized than smaller ones, thus we will define

$$
\begin{aligned}
P_1^c &= \frac{1}{5} \times P_3^c = \frac{1}{5} \\
P_2^c &= \frac{2.5}{5} \times P_3^c = \frac{1}{2} \\
P_3^c &= 1 \qquad \text{(reference power consumption)} \\
P_4^c &= \frac{10}{5} \times P_3^c = 2 \\
P_5^c &= \frac{35}{5} \times P_3^c = 6
\end{aligned}
$$

To handle the distribution of generated power, we will start by looking at the largest windmill parks of Denmark, established as well as scheduled. Among these giants we will consider

[1] Municipalities: Copenhagen $\sim$ 600000, Odense $\sim$ 200000, Aarhus $\sim$ 350000, Average $\sim$ 350000

Anholt Havmøllepark with a total power supply of 400 MW corresponding to a coverage of approximately 400.000 households [4]. The swedish energy company Vattenfall is currently working on another major windmill park, namely Horns Rev 3, which is expected to be finalized in 2020 [8]. This windmill park has a capacity of approximately 406 MW and generates power to about 425.000 households [6]. There are many more parks to consider, and (currently) under construction is also Kriegers Flak windmill park which is predicted to be able to cover almost half a million households and with a power capacity of almost 600 MW [7] [8].

These giant windmill parks will represent our huge generators, and it seems plausible that one of these generators is able to meet the demand of an entire huge consumer (consisting of 350000 households per construction). From this insight we will set the average power generation of a huge generator to

$$P_5^g = P_5^c = 6$$

On the other end of the scale, we will consider some of the smallest windmill parks in Denmark, for instance Vindeby, Tunø Knob, Frederikshavn and Avedøre Holme windmill park with a capacity ranging from 5 MW to 10 MW [8]. These parks will represent our tiny generators. Comparing this power supply with that of one of the giant windmill parks (≈ 400 MW) we expect that our tiny generators can meet the demand of $\frac{5}{400} \times 350000 = 6250$ to $\frac{10}{400} \times 500.000 = 12500$ households.

Since $\frac{12500+6250}{2} \approx 10000$ we will set $P_1^g = P_1^c = \frac{1}{5}$. Finally P_2^g, P_3^g and P_4^g will be be chosen, such that the variance is maximized, this is fulfilled with $P_i^g = \frac{(P_5^g - P_1^g)}{4} \times (i-1) + P_1^g$ for $i = 1, 2, 3, 4, 5$. In particular we have

$$\begin{aligned}
P_1^g &= \frac{1}{5} \\
P_2^g &= \frac{(6 - \frac{1}{5})}{4} \times 1 + \frac{1}{5} = \frac{33}{20} \\
P_3^g &= \frac{(6 - \frac{1}{5})}{4} \times 2 + \frac{1}{5} = \frac{31}{10} \\
P_4^g &= \frac{(6 - \frac{1}{5})}{4} \times 3 + \frac{1}{5} = \frac{91}{20} \\
P_5^g &= 6
\end{aligned}$$

Notice that these values will be adjusted slightly in order to fulfil eq. (5).

This finalizes the construction scheme. Notice that the network size does not appear as an explicit parameter. In fact the size can vary greatly from network to network, but the total power flow remains (approximately) constant.

2.3 Measure normal operation and check for steady state

For each of our simulated network, we will (repeatedly) look for synchronous steady states fulfilling

$$\frac{\mathrm{d}^2\phi_j(t)}{\mathrm{d}t^2} = \frac{\mathrm{d}\phi_j(t)}{\mathrm{d}t} = 0 \qquad \text{for all} \quad j \in \{1, N\} \tag{6}$$

where we recall that $\frac{\mathrm{d}\phi_j(t)}{\mathrm{d}t}$ is the frequency deviation of oscillator j relative to the grid frequency. There exists non-synchronous states which are unwanted, since the transferred power between

two elements is proportional to the sine of their phase difference, thus changing phases leads to oscillations in the power transmission which tend to cancel out over time.

In order to check if our simulated network is in a synchronous steady state we will need a stability measure. To this purpose we introduce the phase order parameter $r(t)$ and the mean square phase velocity $v(t)^2$

$$r(t) := \frac{1}{N}\sum_{j=1}^{N} e^{i\phi_j} \tag{7}$$

$$v(t)^2 := \frac{1}{N}\sum_{j=1}^{N} \left(\frac{\mathrm{d}\phi_j}{\mathrm{d}t}\right)^2 \tag{8}$$

where $|r(t)| \in (0,1)$ reflects the phase coherence and $v(t)^2 \in (0,\infty)$ is self-explanatory.

However rather than using (7) and (8) directly we will prefer to use their long-time averages

$$r_\infty = \frac{1}{T}\lim_{t\to\infty}\int_t^{t+T} \mathrm{d}t' r(t') \tag{9}$$

$$v_\infty^2 = \frac{1}{T}\lim_{t\to\infty}\int_t^{t+T} \mathrm{d}t' v(t')^2 \tag{10}$$

Numerically, t is (of course) finite, but large compared to the oscillation or relaxation period of the system (which will be determined empirically).

In a (ideal) synchronized state we expect that $r_\infty = 1$ and $v_\infty = 0$, therefore we will check that $|r_\infty| > r_{\text{sync}}$ and $v_\infty < v_{\text{sync}}$ for some prescribed constants r_{sync} and v_{sync}.

2.4 Determine critical coupling strength

Each simulated network will operate with a global coupling strength K slightly above the critical capacity K_c, reflecting how most power grids operate [12, p. 2]. That is

$$K = K_c + \epsilon_K \tag{11}$$

To determine the critical coupling strength K_c we will use a bisection algorithm (explained in detail in sec 3.1) where we repeatedly check if the network synchronizes for different values K.

This is done by considering a sample interval $[K_{\min}, K_{\max}]$ and initiate K herein. If this value leads to synchrony, we will restrict ourselves to the interval $[K_{\min}, K]$ and initiate a new value for K. In the opposite case, where there is no synchrony, we will continue our sampling from the top interval $[K, K_{\max}]$. This bisection to smaller and smaller intervals will continue until the interval is *sufficiently* small, in which case we set K to the upper value of this interval. If the interval is small enough, this value of K fulfils (11).

3 Assessing stability characteristic of Type motifs

In the following we will measure two kinds of stability inherent to power systems, namely the *dynamic stability* and the *transient stability*. The first concerns small disturbances in the grid, such as 'natural' fluctuations in the power output/input during a short time interval. The latter examines how the grid responds to larger perturbations (during a long time interval), say if a transmission line gets temporarily deactivated due to a fault.

3.1 Measuring dynamic stability

For the dynamic stability analysis we simulate X networks of Type i-j where $i = 1, 2, 3, 4$ and $j = C, U, R$.

For each node n we will investigate how many times the power output (or input) can be magnified without pushing the system out of synch, denoted m_n from here. This is done by implementing a bisection algorithm outlined below, where we gradually narrow the power (magnification) interval.

For all nodes in all simulated networks of type i-j we will measure the magnification $m_n(g)$ (read 'magnification of node n in grid g'). These quantities relates information concerning the dynamic stability of type i-j networks.

The bisection algorithm
We consider a simulated grid g and node n. Let $M_{\min} \equiv 1$ be the lowest trial magnitude and let $M_{\max}$ be the maximum trial magnitude. This means that if P_n is the power of node n then $M_{\min} \times P_n$ and $M_{\max} \times P_n$ is the lowest and highest power input (or output) respectively that we will consider. $M_{\max}$ is selected such that it is slightly larger than the maximum capacity (among all power lines).

Initially we set $m_n = \frac{M_{\max}+M_{\min}}{2}$ (partitioning the interval in two equal parts) and check if the system resynchronize following this perturbation. If true we know that every magnitude smaller will also synchronize, hence we know that the critical magnitude is found in the top interval. We therefore update the minimum magnitude concordantly $M_{\min} = m_n$ and (re)set $m_n = \frac{M_{\max}+M_{\min}}{2}$ before continuing our search at the top interval. If the system does not synchronize, the critical magnitude is found in the bottom interval and we instead let $M_{\max} = m_n$ before (re)setting $m_n = \frac{M_{\max}+M_{\min}}{2}$.

This search in smaller and smaller intervals terminates when $M_{\max} - M_{\min} < \epsilon$ for some specified ϵ and we report m_n as the critical magnitude.

3.2 Measuring transient stability

The transient stability analysis is carried out using the concept of Basin Stability. Menck *et al.* [10] proposed a component-wise version that we will mirror in the following. Let us outline the idea.

The basin of attraction, denoted $\mathfrak{B}$, constitutes the part of a state space where all trajectories of some dynamical system converge to a particular attractor (a fixpoint in the state space), see

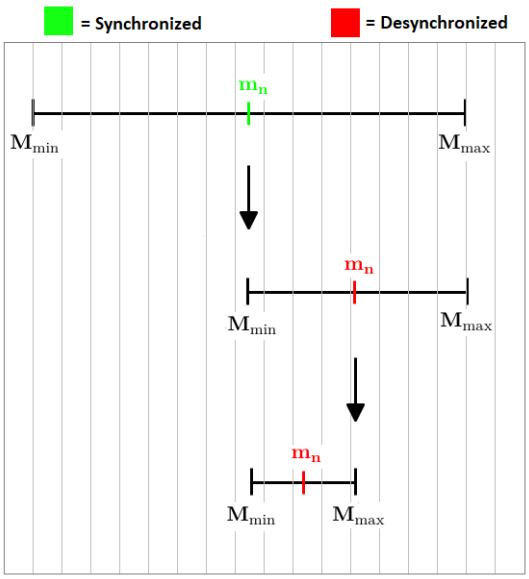

Figure 3: Bisection algorithm: Starting from the full interval (top line) we 'chop' off half the interval (narrowing the line). Which interval we chop is based on whether or not m_n leads to a synchronized state. In the long-run this procedure will converge to the (correct) critical magnitude. Here we have shown an example of three trial magnitudes (three iterations).

figure 4. The basin stability (in the two-dimensional case) will be defined as

$$S(\mathfrak{B}) = \int \mathrm{d}x\mathrm{d}y \mathbb{1}_{\mathfrak{B}}(x,y)\rho(x,y) \tag{12}$$

where ρ is a density of the state space and $\mathbb{1}_{\mathfrak{B}}$ is the indicator function defined as

$$\mathbb{1}_{\mathfrak{B}}(x,y) = \begin{cases} 1 & (x,y) \in \mathfrak{B} \\ 0 & (x,y) \in \mathfrak{B}^c \end{cases}$$

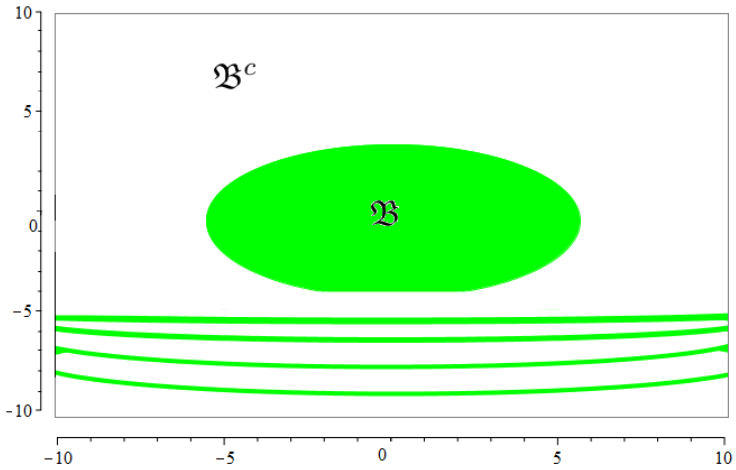

Figure 4: Section of a (two-dimensional) state space $[-10,10] \times [-10,10]$ of some dynamical system. Green area denotes the basin of attraction $\mathfrak{B}$, where trajectories converge to some fixpoint

For our purpose, we will consider a *single node* state space (phase-frequency state space)

$$X_j \equiv \{(\phi_j, \omega_j) \mid (\phi_j, \omega_j) \in [0, 2\pi] \times [-100, 100]\} \tag{13}$$

with $\omega_j \equiv \frac{\mathrm{d}^2\phi_j(t)}{\mathrm{d}t^2}$ and with a uniform density distribution

$$\rho(\phi_j, \omega_j) = \begin{cases} \frac{1}{|X_j|} & (\phi_j, \omega_j) \in X_j \\ 0 & (\phi_j, \omega_j) \notin X_j \end{cases} \tag{14}$$

Now the analysis will progress as follows. During normal operation where all N oscillators operate in synchrony we will have a $2N$-dimensional state space where the system is locked to some fixpoint $(\phi_1^*, \omega_1^*, \phi_2^*, \omega_2^*, ..., \phi_N^*, \omega_N^*)$ in the $2N$-dimensional basin of attraction.

We will now consider generic large perturbations that push a *single* node, say node j, to a new phase-frequency instance (ϕ, ω)

$$(\phi_i, \omega_i) = \begin{cases} (\phi, \omega) & i = j \\ (\phi_i^*, \omega_i^*) & i \neq j \end{cases}$$

This will be repeated for all nodes $j = 1, ..., N$ (keeping the other nodes fixed) and for each node we will measure its *single-node basin stability* S_j defined as

$$S_j \equiv S(\mathfrak{B}_j) \tag{15}$$

where S is the basin stability defined in (12) and $\mathfrak{B}_j$ is the projection of the 2N-dimensional Basin of attraction $\mathfrak{B}$ onto the two-dimensional state space X_j, that is

$$\mathfrak{B}_j = \{(\phi_j, \omega_j) \in X_j \mid (\phi_1, \omega_1, ..., \phi_j, \omega_j, ...\phi_N, \omega_N) \in \mathfrak{B} \text{ and } (\phi_i, \omega_i) = (\phi_i^*, \omega_i^*) \text{ for all } i \neq j\}$$

The single-node basin stability (15) can be estimated numerically by repeatedly drawing pertubations according to the density (14) and observe the number of times the grid resynchronize R_j to the total number of perturbations at node j which will be a fixed number T, thus $S_j \approx \frac{R_j}{T}$.

By simulating multiple grids of the same type and measuring the single-node stability of each node in each grid we will gain insight into the transient stability of the particular class.

3.3 Simulation range using error analysis

Since the number of nodes are not explicit in the construction of the different topologies (Types), simulating a fixed number of grids for each Type would yield Type-specific grids that contain a number of nodes that could vary greatly from grids of a different type. Thus we would not obtain an even number of measurements among each type when doing our (transient and dynamic) analysis, and this would lead to different standard errors and therefore a weak basis on which to make our comparison.

To avoid this we will make a dynamical assessment of the required number of simulations for each type.

Lets start by considering the **transient stability** analysis of some arbitrary topology type. Menck *et al* deduced [17] that measuring one-node basin stability (of node i, say) by drawing T perturbations according to the state space density and counting the number of trajectories that converge to an attractor, denoted R_i, could be viewed as a repeated Bernoulli experiment with standard error

$$e_i = \frac{\sqrt{S_i(1 - S_i)}}{\sqrt{T}}$$

where $S_i \approx \frac{R_i}{T}$ is the one-node basin stability from Monte-carlo sampling.

We might also be interested in the average (one-node) basin stability $S = \frac{1}{N}\sum_{i=1}^{N} S_i$ among the total nodes N with variance

$$\mathrm{Var}(S) = \frac{1}{N^2}\sum_{i=1}^{N}\mathrm{Var}(S_i) = \sum_{i=1}^{N}\frac{e_i^2}{N^2} \tag{16}$$

Since the error falls with the number of nodes we face the problem of a much higher standard error amongst the grid types which exhibits few nodes (such as Type 4), which clouds the comparison of the different types.

To obtain a common standard error would require a uneven number of grid simulations within each type. Lets introduce some new notation. Let $S^{g,t}$ denote the average (one-node) basin stability of simulated grid g within type t. Consider w.l.o.g the two means $S^{g,t}$ and $S^{g',t'}$.

Let G and G' be the number of simulations for each Type respectively. We would now demand that $\mathrm{Var}\left(\frac{1}{G}\sum_{g=1}^{G} S^{g,t}\right) = \mathrm{Var}\left(\frac{1}{G'}\sum_{g'=1}^{G'} S^{g',t'}\right)$ which using (16) leads to

$$\sum_{g=1}^{G}\sum_{i=1}^{N^{g,t}}\frac{{e_i}^{g,t\,2}}{{N^{g,t}}^2 G^2} = \sum_{g'=1}^{G'}\sum_{i=1}^{N^{g',t'}}\frac{{e_i}^{g',t'\,2}}{{N^{g',t'}}^2 G'^2} \tag{17}$$

where $e_i^{g,t}$ is the standard error of node i inside grid g of type t and $N^{g,t}$ are the total number of nodes of simulated grid g of type t.

Numerically, our procedure goes as follows. We pick a threshold value, call it ϵ and perform the transient analysis on Type 1 by simulating a total of G grids until we reach the inequality

$$\sum_{g=1}^{G}\frac{{e_i}^{g,1\,2}}{{N^{g,1}}^2 G^2} \leq \epsilon$$

From here we will just continue our transient analysis on the subsequent Types and enforce (17) (we can now compute one of the sides, since we already simulated Type 1) by dynamically checking if the standard error falls below ϵ. This procedure will lead to an approximate common standard error and a varying number of simulations with respect to each Type.

For the **dynamical stability** analysis we will proceed in the same fashion as we did with the transient. Let $m_i^{g,t}$ be the *magnitude* measurement of node i within grid g of type t.

We then consider a grid-specific mean value $m^{g,t} = \frac{1}{N^{g,t}}\sum_{i=1}^{N^{g,t}} m_i^{g,t}$ and a grid-specific standard error

$$e^{g,t} = \sqrt{\frac{1}{N^{g,t}}\sum_{i=1}^{N^{g,t}}(m^{g,t} - m_i^{g,t})^2}$$

Averaging over all the simulated grids G of type t and all simulated grids G' of type t' and requiring their total variance to be equal we find

$$\mathrm{Var}\left(\frac{1}{G}\sum_{g=1}^{G} m^{g,t}\right) = \sum_{g=1}^{G}\frac{e^{g,t\,2}}{G^2} = \sum_{g'=1}^{G'}\frac{e^{g',t'\,2}}{G'^2} = \mathrm{Var}\left(\frac{1}{G'}\sum_{g=1}^{G'} m^{g',t'}\right) \tag{18}$$

As with the transient analysis, we will begin our dynamical analysis by selecting a ϵ and simulate grids of type 1 until finally $\sum_{g=1}^{G} \frac{e^{g,1}{}^2}{G^2} \leq \epsilon$. We will then continue with the other types and select the simulation size such that (18) is (approximately) fulfilled, which is the case when $\frac{e^{g,t}{}^2}{G^2} \leq \epsilon$.

4 Numerical results

Here we will present the results of our stability analysis. Before moving on we again refer to appendix C for graphical illustrations of the different (instances) type-based networks that we will investigate.

4.1 Dynamical stability analysis

In the dynamical analysis, we set out to measure the number of times the power of any node (of type-specific grids) could be magnified without pushing the system out of synch.

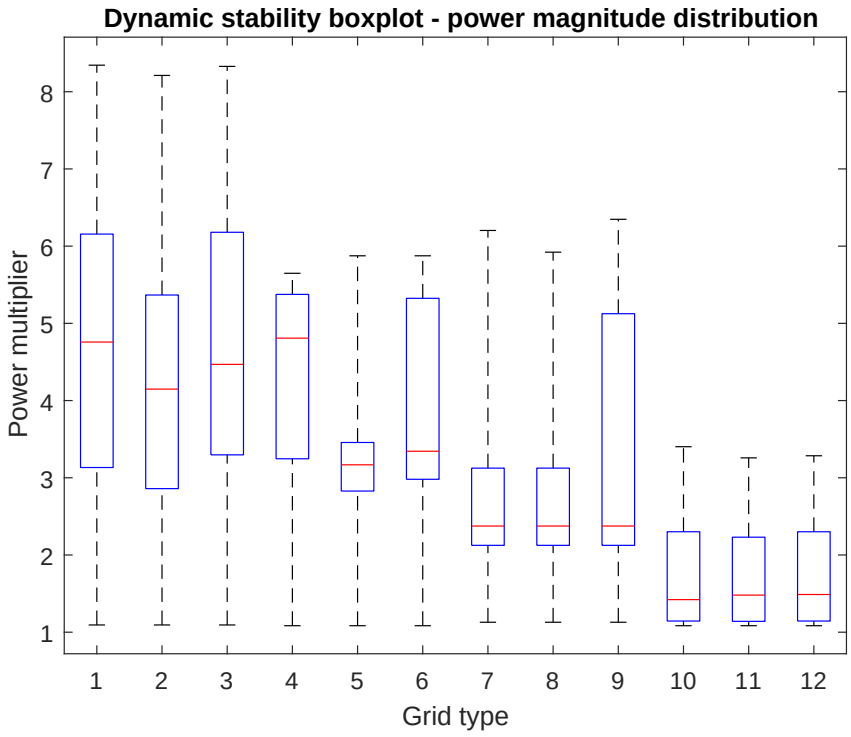

Figure 5: Boxplot over all power magnitude measurements among all simulated grids of a given type. **Grid-type: 'Simulated grids'**. Type 1-C: 3194, Type 1-U: 2938, Type 1-R: 2746, Type 2-C: 4048, Type 2-U: 4145, Type 2-R: 4070 , Type 3-C: 3907, Type 3-U: 3917, Type 3-R: 3903, Type 4-C: 1313, Type 4-U: 1314, Type 4-R: 1292

In total we obtained more than 30000 individual (node-wise) measurements divided among all of the 12 different power grid types.

Their distribution within each type is depicted in the multi-boxplot figure above, see figure 5. In this figure, 'Grid type' 1 corresponds to type $1-C$, 'Grid type' 2 corresponds to $1-U$, 'Grid type' 3 to $1-R$, 'Grid type' 4 to $2-C$, 'Grid type' 5 to $2-U$ and so forward.

From visual inspection we would expect a priori that the topologies of type 1 (i.e. type 1-C, 1-U, 1-R) exhibits a higher dynamic stability measured in terms of how many times the power can be magnified (and thus perturbed) without leading to a limit cycle.

On the other end of the spectrum we find the type 4 topologies with half the measurements pinched in the interval ranging from 1 to (roughly) 2 contrasting the type 1 topologies with half of the measurements in the interval 3 to 6 (roughly).

There's a general tendency that the expected power multiplier (of type specific nodes) decreases with the 'Grid type'. Since the low number 'Grid types' corresponds to grids with few nodes, both on the consumer and generator side, this descend tells us that the larger, more complex and more decentralized power systems are more robust against dynamical fluctuations in agreement with previous findings [12].

As a way of visualizing the *average grid power magnitude* relative to each type, we made type-specific normalplots based on the average power magnitude of every simulated type-specific grid. The result can be seen in figure 6. Also here we notice the pattern, that the expected *average* grid power multiplier seems to shift in the favour of higher dynamical stability as the grid becomes larger with more smaller sources of consumers and generators (type 1). There is no distinctive difference between each subtype (central, uniform, random).

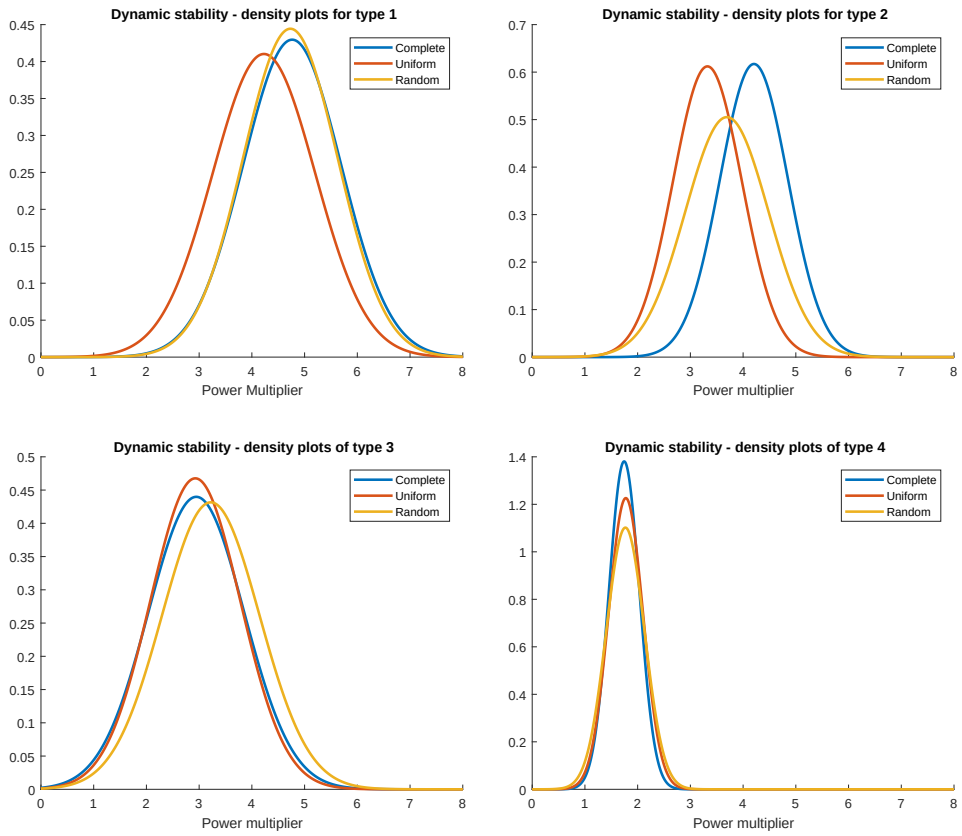

Figure 6: Density plots over type-specific grid-average power magnitude/multiplier. (**mean**, **std. deviation**). Type 1-C : $(4.76, 0.93)$,Type 1-U : $(4.22, 0.97)$, Type 1-R : $(4.73, 0.89)$, Type 2-C : $(4.21, 0.65)$, Type 2-U : $(3.32, 0.65)$, Type 2-R : $(3.69, 0.78)$, Type 3-C : $(2.94, 0.91)$, Type 3-U : $(2.92, 0.85)$, Type 3-R : $(3.22, 0.92)$, Type 4-C : $(1.74, 0.29)$, Type 4-U : $(1.78, 0.33)$, Type 4-R : $(1.76, 0.36)$

In addition to the above, we sought a way to quantify how the distribution of the CBP and GBP, i.e the parameters δ and μ that distributes the total (fixed) power among the different-sized generators and consumers, correlated with the dynamic stability.

To this purpose, we introduced a skewness coefficient, that given a dataset $\mathbf{x}$ is defined as

$$\text{Skewness}(\mathbf{x}) = \frac{\text{mean}(\mathbf{x}) - \text{median}(\mathbf{x})}{\text{standard deviation}(\mathbf{x})} \tag{19}$$

If Skewness < 0 the data is skewed to the right, if Skewness > 0 the data is skewed to the left and if Skewness $= 0$ the data is symmetric. For example, if δ is again the GBP, we expect that Skewness$(\delta) < 0$ for Type 2 and Type 4 (with few large generator), i.e. $\delta \equiv (\delta_1, \delta_2, \delta_3, \delta_4, \delta_5)$ is skewed to the right.

Visualizing the average power magnitude of any grid (i.e. among all types) with a point which size varies with magnitude and plotting this point according to the skewness of the corresponding grids CBP and GBP, we obtained figure 7.

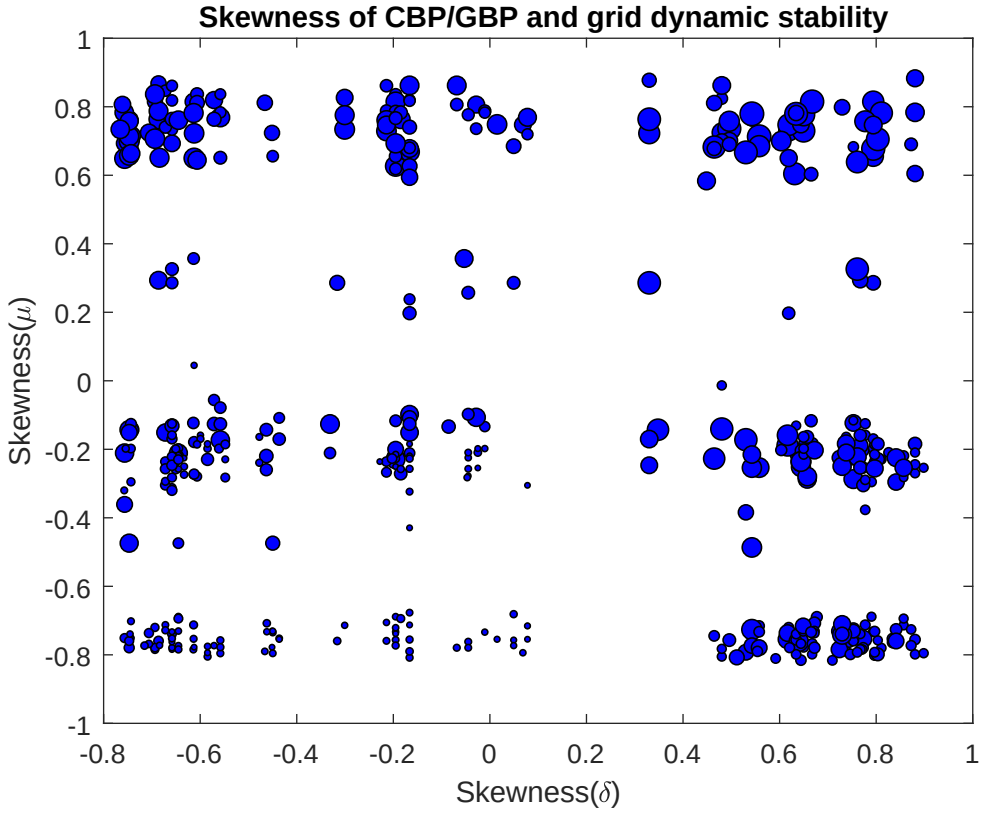

Figure 7: Average power multiplier/magnitude (size of point) for $G = 504$ grids distributed among (all) 12 types.

figure 7 allows us to adopt the concepts and wording of the CBP and GBP in our analysis, parameters that are fundamental for our construction of the power grids. From the figure it is once again apparent that if the CBP and GBP are right skewed (left bottom of the figure), the power magnification reflecting the dynamic stability is lacking. The figure also illustrates that a right-shift in either the CBP or GBP will increase the stability,as we found before. Furthermore it seems probable that a shift in the CBP is preferable to a shift in the GBP, that is replacing huge consumers with many smaller ones seems to have a larger impact than replacing huge generators with many smaller ones. However the combined effect is by far the most eye catching.

4.2 Transient stability analysis

For the transient stability analysis, we used the concept of one-node basin stability to measure how the system responded to large single-node generic perturbations chosen according to the phase-frequency density (14).

As with the dynamic stability analysis, we have chosen to make a multi-boxplot in order to uncover the grid-specific distribution of the one-node basin stability measurements. The result can be seen in figure 8.

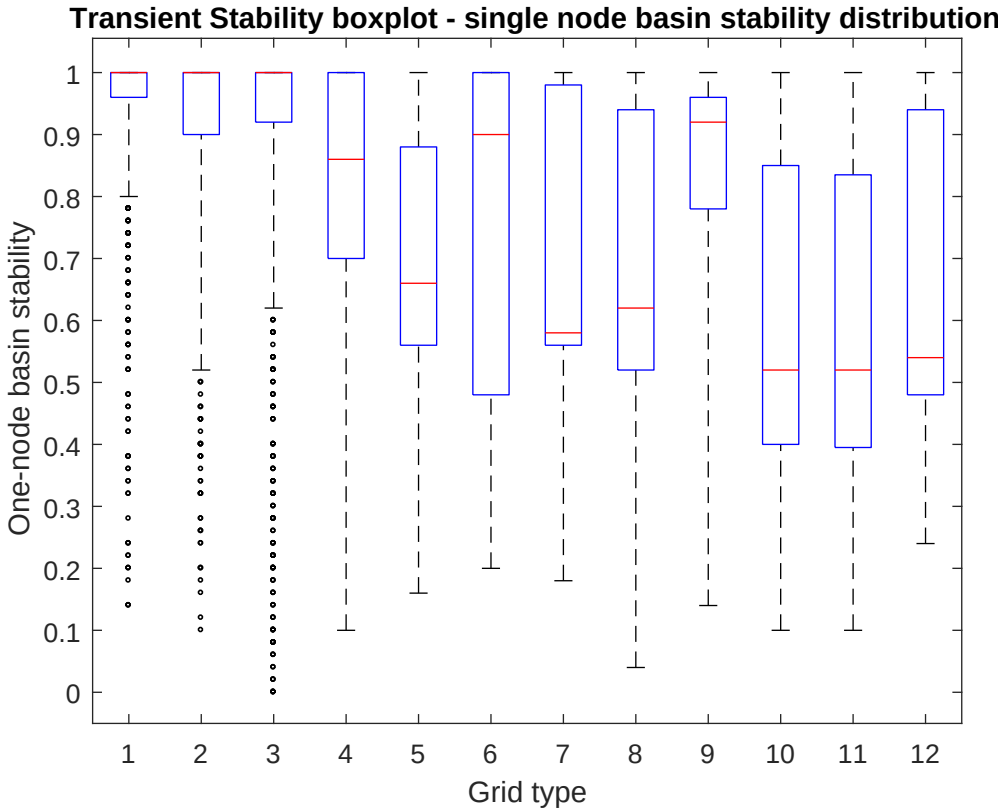

Figure 8: Boxplot over all one-node basin stability measurements among all simulated grids of a given type. Black dots are measurements deemed outliers. **Grid-type: 'Simulated grids'**. Type 1-C: 716, Type 1-U: 985, Type 1-R: 995, Type 2-C: 665, Type 2-U: 331, Type 2-R: 345 , Type 3-C: 298, Type 3-U: 317, Type 3-R: 321, Type 4-C: 136, Type 4-U: 109, Type 4-R: 141

this plot however, unlike the dynamic multi-boxplot, is harder to interpret which in part stems from the fact that the number simulated grids (and thus the number of measurements) is in the low end with roughly 60 simulated grids (and corresponding measurements) - see also section 5 for more of an explanation. The black dots signals outliers (deemed by Matlab) which is also an effect of too few measurements.

Now with this silent warning that the results are not perfectly credible, the boxplots does show a hint that the basin stability seems to fall with the 'Grid type' (defined as before). If true, it also advocates a larger (decentralized) grid with the goal of obtaining a strong power system in terms of transient stability.

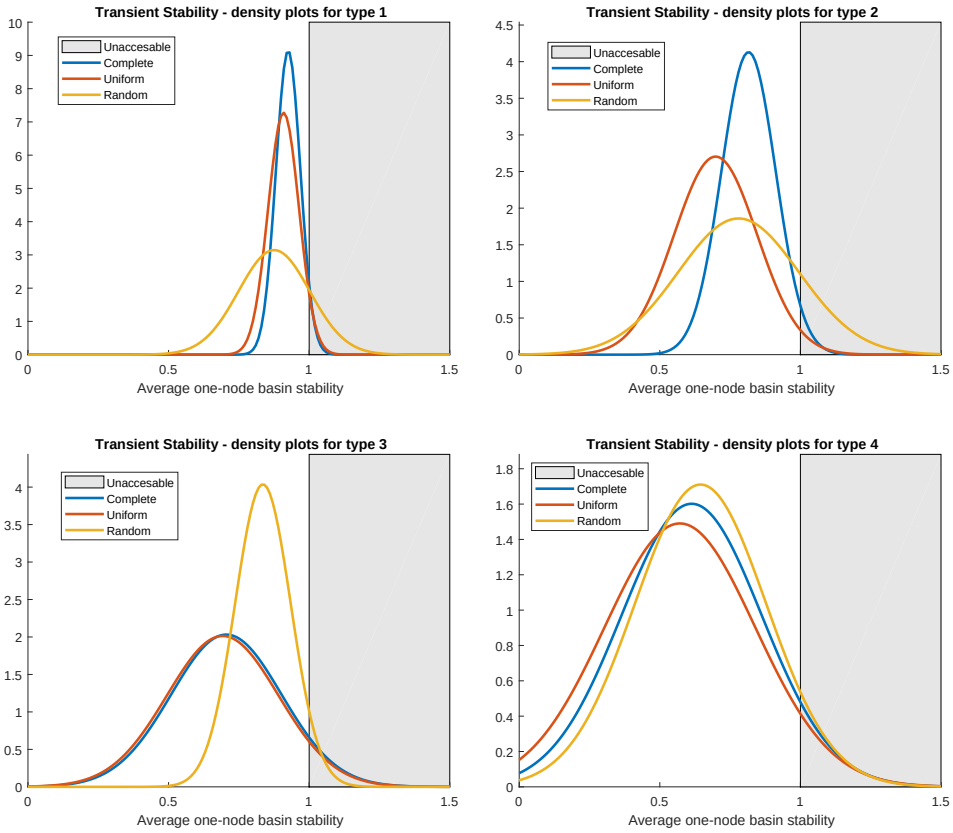

Figure 9: Density plots over type-specific grid-average one-node basin stability.

For each Type, we also simulated a number of grids and calculated the average one-node basin stability. The averages over all grids related to a specific type gave rise to the following 12 type-specific density/normalplots, as seen in figure 9. The grey area simply indicates that one-node basin stability cannot exceed 1. This is in essence just a recast of the picture seen in the multi-boxplot of figure 8. We see the same hint, that Type 1 grids are favourable in terms of basin stability (being shifted far to the right, whereas the other types are more central). We also see that the grids of subtype 'Random' have a (apparent) larger variety of stability states, stated in another way, the collection of (all) grids of subtype 'Random' seem to differ vividly in their basin stability. This is of no large surprise however, since the random grids features all kind of constellations. Otherwise there is no clear difference between any subtypes.

Finally we will, as before, use the concept of the CBP and GBP to analyze the connection between their distribution and the basin stability. Like before we will make use of the skewness measure (19) as explained. Following the same lines, but this time letting the size of the points reflect the average one-node basin stability (of the particular grid), we obtain the plot seen in figure 10.

With this plot it becomes even more clear that there's no safe basis on which to make our conclusion regarding transient stability. Both the upper part and lower part (left aswell as right) is populated by a significant amount of transient stable grids, thus we see no clear inclination as to whether a left-shift or a right-shift of the CBP's and GBP's leads to the most stable choice in regards to larger perturbations.

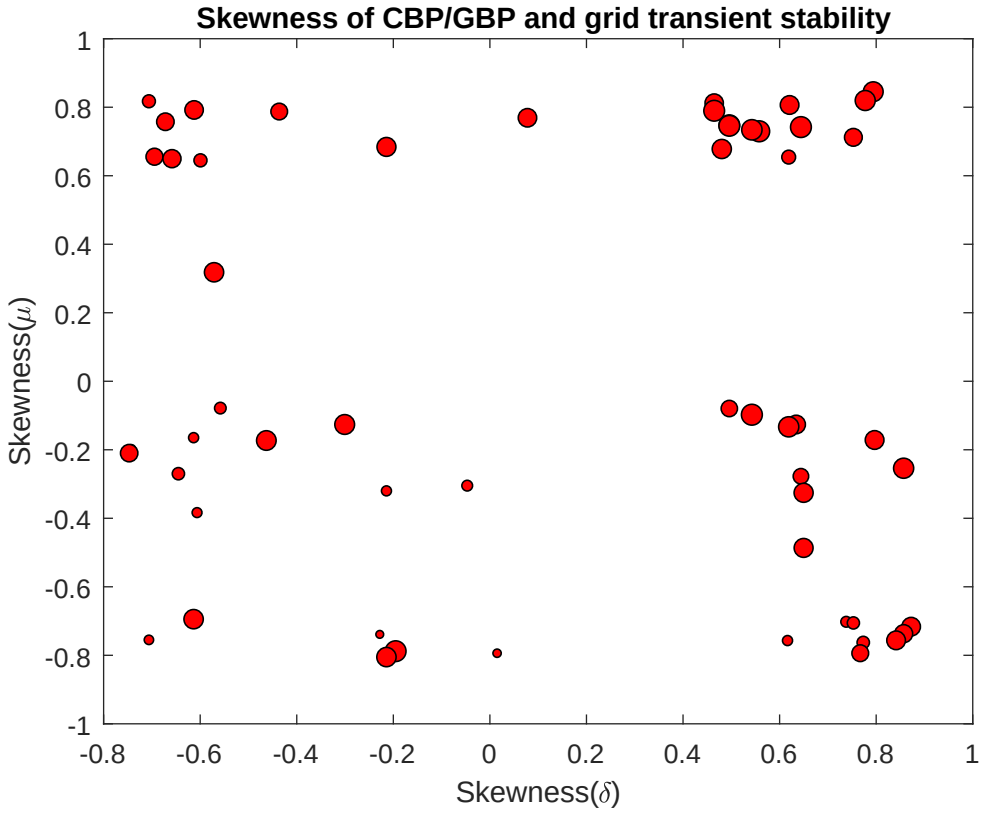

Figure 10: Average one-node basin stability (size of point) for $G = 62$ grids distributed among all (12) types. (**mean**, **std. deviation**). Type 1-C : $(0.93, 0.04)$,Type 1-U : $(0.91, 0.05)$, Type 1-R : $(0.87, 0.13)$, Type 2-C : $(0.81, 0.10)$, Type 2-U : $(0.70, 0.15)$, Type 2-R : $(0.78, 0.21)$, Type 3-C : $(0.71, 0.0.20)$, Type 3-U : $(0.69, 0.20)$, Type 3-R : $(0.83, 0.1)$, Type 4-C : $(0.61, 0.25)$, Type 4-U : $(0.57, 0.27)$, Type 4-R : $(0.64, 0.23)$

5 Discussion and outlook

Using a heuristic construction scheme we were able to construct 12 types or 'classes' of power grids formally denoted 'quasi-isomorphic topologies', each with their own primary type (1,2,3,4) and subtype (Complete,Uniform and Random). The construction divided a (fixed) units of power among 5 size-based types of consumers and generators using parameters known as Consumers balance parameters $\mu \equiv (\mu_1, \mu_2, \mu_3, \mu_4, \mu_5)$ and Generator balance parameters $\delta \equiv (\delta_1, \delta_2, \delta_3, \delta_4, \delta_5)$. The size of the network (n.o. consumers and generators) were not explicit in this construction, instead the procedure allowed us to investigate how the distribution of power among different types of units influence the stability of the power grid. The large complex grids and the small simple grids, aswell the decentralized (few generators) and centralized grids were all implicitly build into assortment of type-grids.

Our task was to examine how the different power grids of each type responded to changes in the power flow. In particular we examined the dynamical and transient stability by power magnification method and a one-node basin stability method respectively.

While we did not necessarily aim to uncover a difference in stability between the different types,

the realizations that the subtypes could barely be distinguished in both stability analysis made us question if the separation/classification of the power grid types might have been too 'weak'. On the other hand, showing a number of types is indistinguishable is also something.

We did succeed in showing that the dynamic stability is highly correlated to the size and decentralization of the network, as previously reported.

Unfortunately, the transient stability analysis was far from as successful. The numerical workload was enormous, and the time restriction made it impossible to harvest enough results for a sensible analysis which is visible in the plots and figures of the transient analysis section. This is above all a personal misjudgement from the (main)author of this paper.

In retrospect we managed to construct and classify a portion of highly relevant power grids given the constantly changing complexity of modern power grids. While the structure of the type-specific grids did not add anything *new* to the table, we did however succeed in producing results in accordance with similar studies within this area.

With more time at hand, it would be interesting to scrutinize the construction scheme and refine it by constructing more elaborate power grid designs with structural parameters (i.e. depth, symmetry, sparsity etc.) and investigate in more details how the construction affects the synchronous operation of the power system.

A Constructing Quasi-isomorphic topologies

In the construction scheme we seek to define types based on the CBP and GBP, that is the μ_i and δ_i, such that the CBP and GBP on average tend to decrease (or increase) with i.

Stated formally, on average we demand that $\mu_1 < \mu_2 < \mu_3 < \mu_4 < \mu_5$ or with reversed inequalities (depending on the type) and likewise for δ_i (depending on the type). The types are in a general sense defined such that

Type 1, on average, fulfils $\mu_i < \mu_{i+1}$ and $\delta_i < \delta_{i+1}$.
Type 2, on average fulfils $\mu_i < \mu_{i+1}$ and $\delta_i > \delta_{i+1}$.
Type 3, on average, fulfils $\mu_i > \mu_{i+1}$ and $\delta_i < \delta_{i+1}$.
Type 4, on average, fulfils $\mu_i > \mu_{i+1}$ and $\delta_i > \delta_{i+1}$.

The average of the CBP and GBP is captured in the array $\Lambda \equiv \{\Lambda_1, \Lambda_2, \Lambda_3, \Lambda_4, \Lambda_5\} = \{0.5, 0.2, 0.15, 0.1, 0.05\}$. For type 1, this means that

$$(\bar{\delta_1}, \bar{\delta_2}, \bar{\delta_3}, \bar{\delta_4}, \bar{\delta_5}) = \Lambda = (\bar{\mu_1}, \bar{\mu_2}, \bar{\mu_3}, \bar{\mu_4}, \bar{\mu_5})$$

where $\bar{\delta_i}$ is the average of δ_i and likewise $\bar{\mu_i}$ is the average of μ_i.

For type 2 however the inequalities are flipped for the δ_i so the mean instead becomes

$$(\bar{\delta_5}, \bar{\delta_4}, \bar{\delta_3}, \bar{\delta_2}, \bar{\delta_1}) = \Lambda = (\bar{\mu_1}, \bar{\mu_2}, \bar{\mu_3}, \bar{\mu_4}, \bar{\mu_5})$$

To add randomness in the distribution of the CBP and GBP while at the same time ensuring that Λ does in fact represents the mean, we introduce the array of deviations $\lambda \equiv \{\lambda_{12}, \lambda_{23}, \lambda_{34}, \lambda_{45}\} = \{0.2, 0.1, 0.1, 0.05\}$.

Now the sampling process proceeds as follows. Without loss of generality, lets focus on type 3. We randomly assign δ_1 to a value in the interval $[\Lambda_1 - \lambda_{12}, \Lambda_1 + \lambda_{12}]$.
With δ_1 picked, we will adjust the sampling space of δ_2 by $\Lambda_1 - \mu_1$ (notice this could be negative), see figure 11. Thus δ_2 is randomly assigned to a number in the interval $[\Lambda_2 + \Lambda_1 - \delta_1 - \lambda_{23}, \Lambda_2 + \Lambda_1 - \delta_1 + \lambda_{23}]$.
Likewise the sampling space of δ_3 is adjusted after the selection of δ_2. Once $\delta_1, \delta_2, \delta_3, \delta_4$ are selected, δ_5 is also given, by demanding that $\sum_{j=1}^{5} \delta_j = 1$.

For type 3 the inequalities are flipped for the μ_i. To ensure that the mean array Λ is also 'reversed' (such that $\bar{\mu_5} = \Lambda_1$, $\bar{\mu_4} = \Lambda_2$ and so forth) we simply change the sampling order, such that μ_5 (instead of μ_1) is selected from the interval $[\Lambda_1 - \lambda_{12}, \Lambda_1 + \lambda_{12}]$ and μ_4 is then selected from $[\Lambda_1 + \Lambda_2 - \mu_5 - \lambda_{23}, \Lambda_1 + \Lambda_2 - \mu_5 + \lambda_{23}]$ and so forth, until finally $\mu_1 = 1 - \sum_{j=2}^{5} \mu_j$.

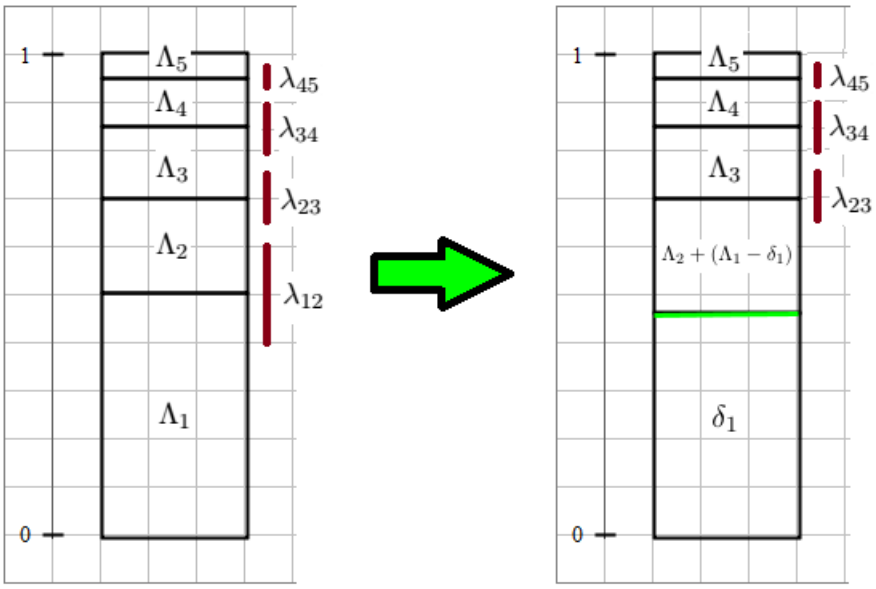

Figure 11: Selection of δ_1 and the increase in sampling space of δ_2

B Deriving the grid model

Consider a power grid consisting of N synchronous (rotating) machines. Each machine represents a generator or consumer. The power grid usually runs at a utility frequency of 50 Hz, which gives us a utility *angular* frequency of $\Omega = 2\pi \times 50$ Hz. The frequency could also be taken as 60 Hz depending on the power grid in question.

If we consider an arbitrary machine j and let $\phi_j(t)$ denote the deviation from the net frequency, we can write the mechanical phase as:

$$\theta_j(t) = \Omega t + \phi_j(t)$$

which is synchronized with the supply current. For any machine j, we can use the law of energy conservation to determine the consumed or generated power:

$$P_j^{mach} = P_j^{acc} + P_j^{diss} + \sum_{i=1}^{N} P_{ij}^{trans}$$

Here P_j^{mach} is the power at machine j, $P_j^{acc} = \frac{1}{2} I_j \frac{d}{dt}(\dot{\theta}_j)^2 = I_j \ddot{\theta}_j \dot{\theta}_j$ is the rate at which kinetic rotational energy is accumulated in the machine, $P_{ij}^{diss} = \kappa_j (\dot{\theta}_j)^2$ is the rate of energy dissipation due to friction and finally $P_{ij}^{trans} = P_{ij}^{max} \sin(\phi_i - \phi_j)$ denotes the rate at which energy is surging from machine i to machine j.

Notice the crude assumption that energy dissipation is only due to friction, ignoring ohmic loss etc.

Inserting the relevant quantities we obtain:

$$\begin{aligned} P_j^{mach} &= I_j \ddot{\theta}_j \dot{\theta}_j + \kappa_j (\dot{\theta}_j)^2 + \sum_{i=1}^{N} P_{ij}^{max} \sin(\phi_i - \phi_j) \\ &= I_j \ddot{\phi}_j (\Omega + \dot{\phi}_j) + \kappa_j (\Omega + \dot{\phi}_j)^2 + \sum_{i=1}^{N} P_{ij}^{max} \sin(\phi_i - \phi_j) \\ &= I_j \Omega \ddot{\phi}_j + I_j \ddot{\phi}_j \dot{\phi}_j + 2\kappa_j \Omega \dot{\phi}_j + \kappa_j \dot{\phi}_j{}^2 + \kappa_j \Omega^2 + \sum_{i=1}^{N} P_{ij}^{max} \sin(\phi_i - \phi_j) \\ &:= f(\dot{\phi}_j) \end{aligned} \tag{20}$$

Under the assumption that each rotating machine operates close to the utility frequency ($\dot{\phi}_j \ll \Omega$) we obtain the following 1st order approximation:

$$\begin{aligned} f(\dot{\phi}_j) &\approx (I_j \Omega \ddot{\phi}_j + \kappa_j \Omega^2 + \sum_{i=1}^{N} P_{ij}^{max} \sin(\phi_i - \phi_j)) + (I_j \ddot{\phi}_j + 2\kappa_j \Omega) \dot{\phi}_j \\ &\approx I_j \Omega \ddot{\phi}_j + \kappa_j \Omega^2 + 2\kappa_j \Omega \dot{\phi}_j + \sum_{i=1}^{N} P_{ij}^{max} \sin(\phi_i - \phi_j) \end{aligned}$$

In the last line we used that the rate at which kinetic energy accumulates is significantly lower than the rate at which energy dissipate ($I\Omega\ddot{\phi} \ll \kappa\Omega^2$), which is a sensible assumption for mechanical systems (see [18, sec.2, eq. (11)]).

Comparing the approximation with (20) and omitting the weak inequality sign we obtain:

$$P_j^{mach} = I_j \Omega \ddot{\phi}_j + \kappa_j \Omega^2 + 2\kappa_j \Omega \dot{\phi}_j + \sum_{i=1}^{N} P_{ij}^{max} \sin(\phi_i - \phi_j) \tag{21}$$

Dividing through by $I\Omega$ and defining the new standard variables $P_j = \frac{P_j^{mach} - \kappa_j \Omega^2}{I_j \Omega}$, $\alpha_j = 2\kappa_j \Omega$, $K_{ij} = \frac{P_{ij}^{max}}{I_j \Omega}$ we can rearrange (21) and recognize the leading equation of the kuramato-like model

$$\ddot{\phi}_j = P_j - \alpha_j \dot{\phi}_j + \sum_{i=1}^{N} K_{ij} \sin(\phi_i - \phi_j)$$

From the final equation, we observe that the dynamics of the system depends not on the phases θ_j but only on their deviation from the utility frequency and their mutual difference.

C Visualizing grid types

Red squares symbol generators while blue dots symbols consumers.

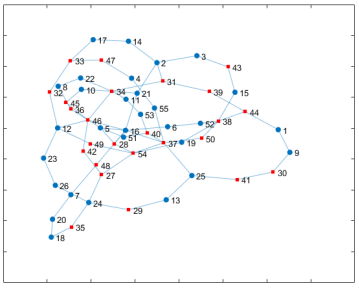

(a) Type 1-C

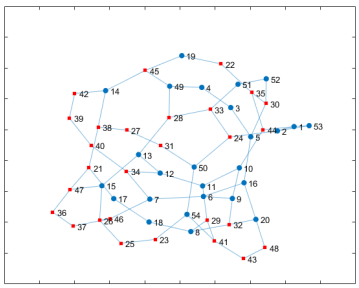

(b) Type 1-U

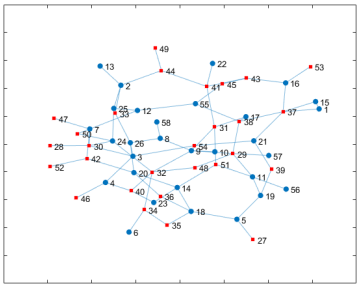

(c) Type 1-R

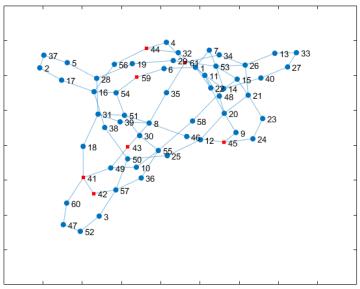

(d) Type 2-C

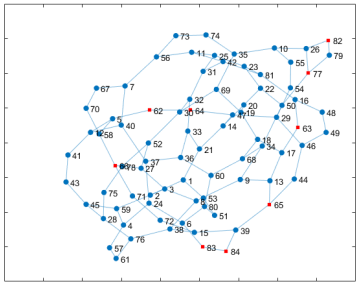

(e) Type 2-U

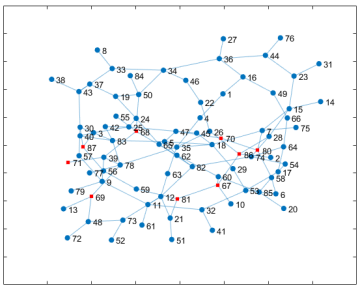

(f) Type 2-R

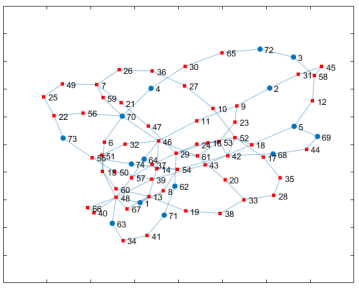

(g) Type 3-C

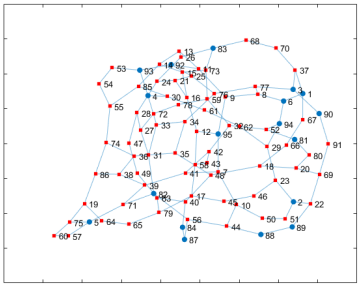

(h) Type 3-U

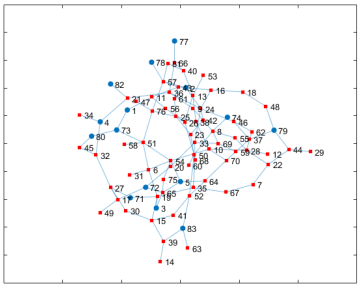

(i) Type 3-R

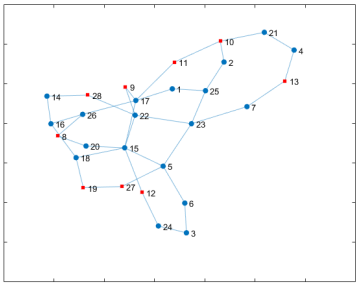

(j) Type 4-C

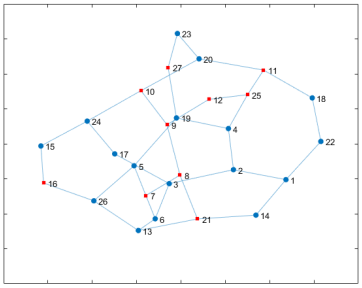

(k) Type 4-U

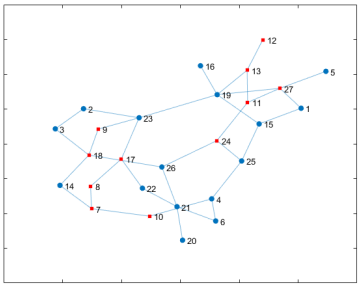

(l) Type 4-R

References

[1] Energinet.dk: det danske transmissionsnet, http://energinet.dk/DA/El/Nyheder/Sider/Nu-kan-du-downloade-data-om-det-danske-elsystem-i-2020.aspx, retrieved 14-05-2016

[2] J Nitzbon et al 2017 New J. Phys. 19 033029 DOI: 10.1088/1367-2630/aa6321

[3] SparEnergi.dk: beregn dit energiforbrug, https://sparenergi.dk/forbruger/el/dit-elforbrug, retrieved 29-12-2017

[4] DongEnergy.dk: Anholt Havmøllepark, http://www.dongenergy.com/da/vores-forretning/wind-power/hvor-vi-er-aktive/anholt, retrieved 29-12-2017

[5] Ingeniøren.dk: Et af danmarks største kraftværker lukker (næsten) elproduktionen, https://ing.dk/artikel/et-af-danmarkshistoriens-stoerste-kraftvaerker-lukker-naesten-elproduktionen-181164, retrieved 29-12-2017

[6] Ingeniøren.dk: 200 kæmpevindmøller ved Møn skal levere strøm til 500.000 hustande, https://ing.dk/artikel/200-kaempevindmoller-ved-mon-skal-levere-strom-til-500000-husstande-116106, retrieved 29-12-2017

[7] tvsyd.dk: Danmarks største vindmøllepark skal give el til 425.000 danske hjem, retrieved 29-12-2017

[8] Energistyrelsen: eksisterende havmølleparker, https://ens.dk/ansvarsomraader/vindenergi/eksisterende-havvindmoelleparker-og-aktuelle-projekter, retrieved 29-12-2017

[9] Danmarks Statistik: Folketal 1.jan efter byområde (...), http://www.statistikbanken.dk/BY1, retrieved 28-12-2017

[10] Menck, P. J. et al. How dead ends undermine power grid stability. (2014). Nat. Commun. 5:3969 DOI: 10.1038/ncomms4969

[11] Dirk Witthaut and Marc Timme 2012 New J. Phys. 14 083036 DOI: 10.1088/1367-2630/14/8/083036

[12] M. Rohden, A. Sorge, D. Witthaut and M.Timme. (2012). Self-organized synchronization in Decentralized Power Grids. Physical Review Letters 109(6):064101 DOI: 10.1103/PhysRevLett.109.064101

[13] M. Rohden, A. Sorge, D. Witthaut and M. Timme. (2014). Impact of network topology on synchrony of oscillatory power grids. Chaos. 2014 Mar;24(1):013123 DOI: 10.1063/1.4865895.

[14] Benjamin Schäfer et al 2015 New J. Phys. 17 015002 DOI:10.1088/1367-2630/17/1/015002

[15] H. Kim, S.H. Lee, P. Holme. (2016). Building blocks of the basin stability of power grids. Physical Review E 93(6):062318. DOI: 10.1103/PhysRevE.93.062318

[16] Energistyrelsen: Smart Grid-Strategi (fremtidens intelligente energisystem), https://ens.dk/sites/ens.dk/files/EnergiKlimapolitik/smart_grid-strategi-2.pdf, retrieved 05-04-2018

[17] P.J. Menck, J. Heitzig, N. Marwan, J. Kurths.(2013). How basin stability complements the linear-stability paradigm. Nature Physics 9(2):89-92 DOI: 10.1038/nphys2516

[18] Filatrella, G., Nielsen, A. & Pedersen, N. Eur. Phys. J. B (2008) 61: 485 DOI: 10.1140/epjb/e2008-00098-8

[19] Nielsen, L.R. (2016). Stability analysis of power grid topologies. Non-published.